PAPER

Probing wavepacket dynamics using ultrafast x-ray spectroscopy

IOP Publishing Journal of Physics B: Atomic, Molecular and Optical Physics

J. Phys. B: At. Mol. Opt. Phys. **48** (2015) 214001 (11pp) doi:10.1088/0953-4075/48/21/214001

Probing wavepacket dynamics using ultrafast x-ray spectroscopy

G Capano[1], C J Milne[2], M Chergui[1], U Rothlisberger[3], I Tavernelli[4] and T J Penfold[2]

[1] Ecole polytechnique Fédérale de Lausanne, Laboratoire de spectroscopie ultrarapide, ISIC, FSB, CH-1015 Lausanne, Switzerland
[2] SwissFEL, Paul Scherrer Inst, CH-5232 Villigen, Switzerland
[3] Ecole polytechnique Fédérale de Lausanne, Laboratoire de chimie et biochimie computationnelles, ISIC, FSB-BSP, CH-1015 Lausanne, Switzerland
[4] IBM Research GmbH, Zurich Research Laboratory 8803 Rueschlikon, Switzerland

E-mail: tom.penfold@ncl.ac.uk

Received 27 May 2015, revised 6 July 2015
Accepted for publication 17 July 2015
Published 23 September 2015

Abstract

The advent of x-ray free electron lasers is providing new opportunities for probing the ultrafast excited state dynamics using structurally sensitive techniques. Herein we use excited state wavepacket dynamics of a prototypical Cu(I)-phenanthroline complex, $[Cu(dmp)_2]^+$ (dmp = 2, 9-dimethyl-1, 10-phenanthroline) to investigate how femtosecond vibrational and electronic relaxation is translated into transient x-ray absorption and emission. Using realistic experimental parameters we also derive the anticipated signal strengths for these transient features. This indicates that although recording a signal capturing the strongest transient (i.e. excited state–ground state) changes will be possible for all cases, only with x-ray absorption near-edge structure and extended x-ray absorption fine structure will it be possible to resolve the fine details associated with the wavepacket dynamics within realistic experimental acquisition times.

S Online supplementary data available from stacks.iop.org/jpb/48/214001/mmedia

Keywords: femtosecond, x-ray spectroscopy, wavepacket dynamics, x-ray free electron lasers, excited state dynamics

(Some figures may appear in colour only in the online journal)

1. Introduction

Probing ultrafast non-equilibrium dynamics became possible with the advent of ultrafast time-resolved linear and non-linear optical spectroscopies [1, 2]. However, because optical spectroscopy consists of transitions between delocalized valence states, the link between the spectroscopic observable and structure is ambiguous for systems of more than one nuclear degree of freedom, i.e. >2 atoms. To overcome this, the last decades have witnessed a significant research effort aimed at exploiting short wavelength probe pulses to achieve direct structural sensitivity in time-resolved pump–probe experiments. This has led to the development of time-resolved diffraction methods using x-rays [3–5] or electrons [6, 7] and core level spectroscopies using either x-rays [8–11] or electrons [12, 13].

For the implementation of time-resolved x-ray spectroscopy, the focus of this present work, third generation light sources are most suited because of their wide tuneability, stability and high photon flux. However, for normal operational modes, the x-ray pulses from these light sources have a temporal width of 50–100 ps. They are therefore unable to probe the initial ultrafast dynamics that can often be critical in determining the outcome of non-equilibrium dynamics. While this can, to a certain extent, be overcome using the laser-slicing scheme [14] which has been used to demonstrate femtosecond x-ray spectroscopy [15–18], these experiments are extremely challenging due to low photon counts. With an x-ray flux per pulse that is typically 10–11 orders of

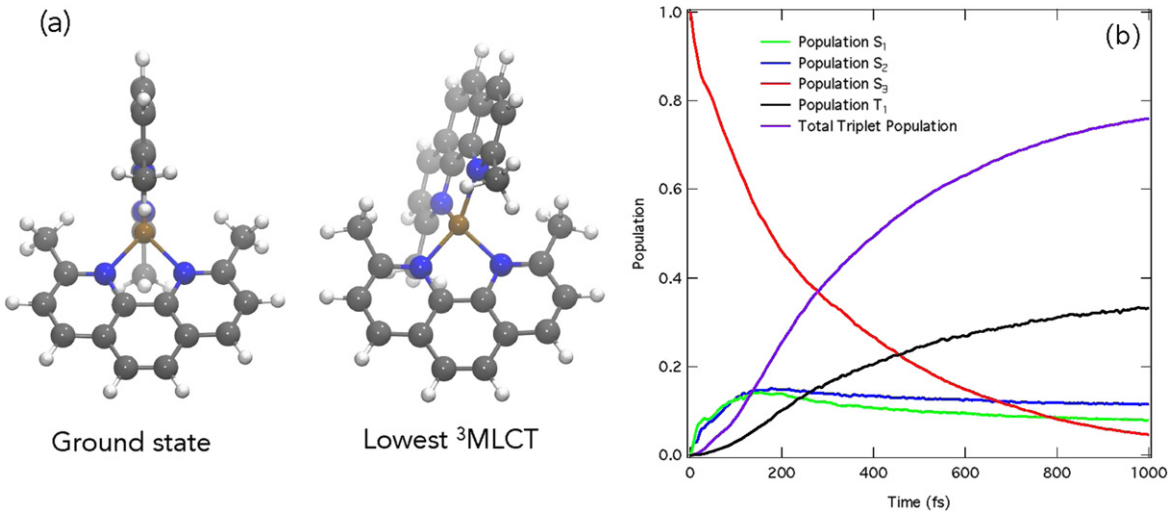

Figure 1. (a) DFT (B3LYP)-optimized geometry of the ground state (left) and lowest triplet state (right) of $[Cu(dmp)_2]^+$. (b) Relative diabatic state populations of S_1 (blue), S_2 (green), S_3 (red), T_1 (black) and all the triplet (T1–T4) states (purple), for 1 ps following photoexcitation. Figure replotted from [28].

magnitude higher than the laser-slicing scheme, x-ray free electron lasers (X-FELs) [19] offer new perspectives for performing ultrafast x-ray experiments. Indeed, femtosecond x-ray spectroscopy at X-FELs has been demonstrated for photoexcited $[Fe(bpy)_3]^{2+}$ [20, 21], $[Fe(phen)_2(NCS)_2]$[22] $[Fe(C_2O_4)_3]^{3-}$ [23] and $Fe(CO)_5$ [24].

These studies have been used to shed light into the evolving electronic structure, changing spin states and overall structural changes occurring after photoexcitation. However, none of these studies have probed the nuclear wavepacket dynamics, which is commonly elucidated from femtosecond optical spectroscopy [25, 26]. Indeed directly observing signatures of (coherent) vibrational dynamics, electronic relaxation, intramolecular energy redistribution and vibrational cooling can shed important insight into how a particular system dissipates the energy after photoexcitation. Consequently, the absence of these dynamics in any time-resolved x-ray spectroscopic experiment reported to date poses a number of questions (i) What is the sensitivity of x-ray spectroscopic techniques to wavepacket dynamics? (ii) What is the measurement sensitivity and therefore number of photons required to successfully observe these dynamics? (iii) What is the best x-ray spectroscopic technique to observe these dynamics?

To address these questions, in this paper we use first principles quantum dynamics simulations [27, 28] of a prototypical Cu(I)-phenanthroline complex, $[Cu(dmp)_2]^+$ (dmp = 2, 9-dimethyl-1, 10-phenanthroline), initiated after photoexcitation into the optically bright metal-to-ligand charge-transfer (MLCT) state to investigate how femtosecond nuclear wavepacket dynamics are reflected in x-ray spectroscopic signals. This is achieved by studying the extended x-ray absorption fine structure (EXAFS), pre-edge x-ray absorption near-edge structure (XANES), $K\alpha_{1,2}$, $K\beta_{1,3}$ and $K_{\beta_{2,5}}$ (sometimes referred to as valence-to-core) x-ray emission (XES) spectra. Subsequently, using realistic experimental parameters we derive the anticipated signal strengths for these transient (i.e. excited state–ground state) features. For the present complex, these simulations show that while recording a signal capturing the strongest transient changes is possible for each spectroscopic method, only for XANES and EXAFS will it be possible to resolve the fine details associated with wavepacket dynamics within realistic experimental acquisition times.

2. Theory and computational details

2.1. Quantum dynamics of $[Cu(dmp)_2]^+$

In this work we derive ultrafast x-ray spectroscopic signals from our recent quantum dynamics of a prototypical Cu(I)-phenanthroline complex, $[Cu(dmp)_2]^+$ [27, 28]. The ultrafast dynamics of $[Cu(dmp)_2]^+$ have previously been well characterized using optical absorption and emission spectroscopies [29–34]. The general picture that emerges from these studies indicates that following photoexcitation, the complex relaxes into the lowest singlet excited state in ~100 fs. This is followed by a structural distortion (flattening of the dihedral angle between the ligands, see figure 1(a)), and intersystem crossing (ISC) to the lowest triplet state T_1 [34]. Of particular relevance to the present work, Tahara and co-workers [32–34] have demonstrated the presence of distinct wavepacket dynamics occurring in the excited state. These coherent vibrational dynamics are dominated by a vibrational mode with frequency 125 cm^{-1} (period of ~300 fs), which was assigned to a breathing mode of the complex that causes a symmetric stretching of the four Cu–N bonds [33].

The quantum dynamics used herein are presented in detail in [27, 28] and were performed using the Heidelberg multi configuration time dependent hartree package [35, 36]. The Hamiltonian was described using the vibronic coupling model [37]. It included eight nuclear degrees of freedom, the three lowest singlet states and the four lowest triplet states

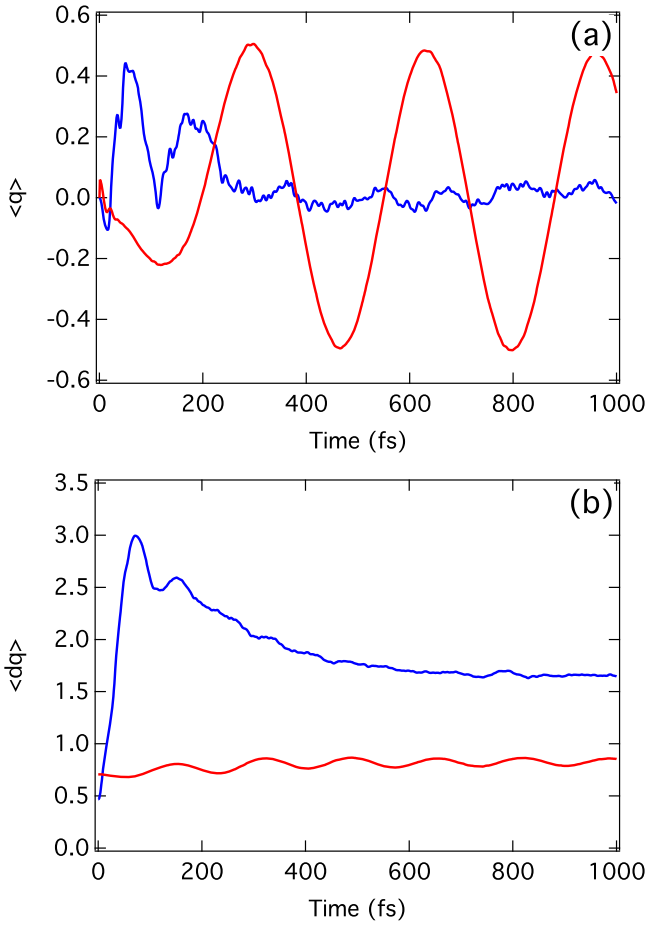

Figure 2. Expectation value of the position, $\langle q \rangle$ (a), and of the width, $\langle dq \rangle$ (b), of the wavepacket in the T_1 state. Colors: red, ν_8; blue, ν_{21}.

[27]. The population kinetics during the first picosecond after photoexcitation are shown in figure 1(b). After photoexcitation, which populates the S_3 state (red trace, figure 1(b)), we observe rapid population decay into the S_2 and S_1 states. Due to a degeneracy of these states with the lowest lying triplet states, there is rapid ISC into the triplet manifold (purple line) and after 1 ps ~80% of the wavepacket is in the triplet states. Of this population, just under half is in the T_1 state. Further details of the quantum dynamics simulations used in this study can be found in [27, 28].

As discussed below, much of this study focuses upon the dynamics along modes ν_8 and ν_{21} in the T_1 state. ν_8 is the totally symmetric breathing mode responsible for the contraction of the Cu–N distance in the excited state and ν_{21}, is the mode associated with the pseudo Jahn–Teller (PJT) distortion. Figure 2 shows the position and width of the wavepacket in the T_1 state along these modes. The position of the wavepacket along ν_8 shows an oscillation with a period of ~300 fs in good agreement with the wavepacket dynamics reported by Tahara *et al* [55], The width only shows small oscillators, and remains roughly constant throughout the first picosecond. In contrast, ν_{21} exhibits no significant displacement from the Franck–Condon geometry. Instead, due to the vibrationally hot nuclear wavepacket, in these states the dynamics are reflected in the width of the wavepacket, rather than position. Here, at early times we observe a large increase in the width of the wavepacket along ν_{21}. The gradual decrease in this width is highlighting the beginning of vibrational relaxation.

2.2. Simulations of the time-resolved spectra

The x-ray spectrum of the non-stationary wavepacket is calculated as the weighted sum of the spectra calculated at each grid point used to describe the nuclear wavepacket. The weighting corresponds to the magnitude of the nuclear wavepacket at that grid point. For the EXAFS spectra, a sum over each electronic state was also performed, thus achieving a description of the full nuclear wavepacket. All of the other spectra (pre-edge XANES and XES) only considered the wavepacket, and thus the dynamics, on the T_1 state.

This is because, in contrast to EXAFS spectra, the valence electronic structure is expected to influence the spectrum, meaning that for the excited states (i.e. S_1, S_2, S_3 and T_2, T_3, T_4), one must simulate the core-level spectrum of each excited state. Due to the two excitation steps, the transition dipole matrix elements between the valence excited state and the final core-excited state cannot be computed within linear response theories, such as linear response-time-dependent density functional theory. However, since DFT is rigorously valid for the lowest state of a given spin, we are able to simulate the T_1 state.

At present, the most rigorous approach of simulating the core-level spectra of electronically excited states is restricted active space self consistent field method [38]. However, since these calculations are extremely computationally intensive they are unrealistic to describe the time-evolution of a nuclear wavepacket. Consequently, this approach is best applied to probe selected important points of the dynamics, as recently demonstrated in the study of photoexcited $Fe(CO)_5$ [24]. An alternative approximate way to address the excited state is using a ΔSCF approach, such as the maximum overlap method [39, 40]. However, this requires that the excited state is well describe by a single electron excitation, such as a HOMO–LUMO transition. Unfortunately this is not the case for the present system. In addition, the character of the excited states changes along the main reaction path making it impossible to assign a single configuration to represent each of the excited states.

The EXAFS spectra at each grid point were calculated with the FEFF9 package [41] using the path expansion multiple scattering approach and a self-consistent field (SCF) potential. All scattering pathways shorter than 6 Å were included. The x-ray absorption (XAS) and XES spectra were computed within the one-electron approach [42, 43] as implemented in the ORCA [44] quantum chemistry package. Computations used the BP86 functional [45, 46] and the def2-TZVP basis set [47, 48]. All of the calculations included spin–orbit coupling (SOC), for which the SOC operator is approximated by the spin–orbit mean field method (SOMF) [49]. A Lorentzian lifetime broadening with full-width half maximum (FWHM) of 1.89 eV was applied to the pre-edge XANES, while a Lorentzian broadening with FWHM of 2.5 eV was used for the XES spectra.

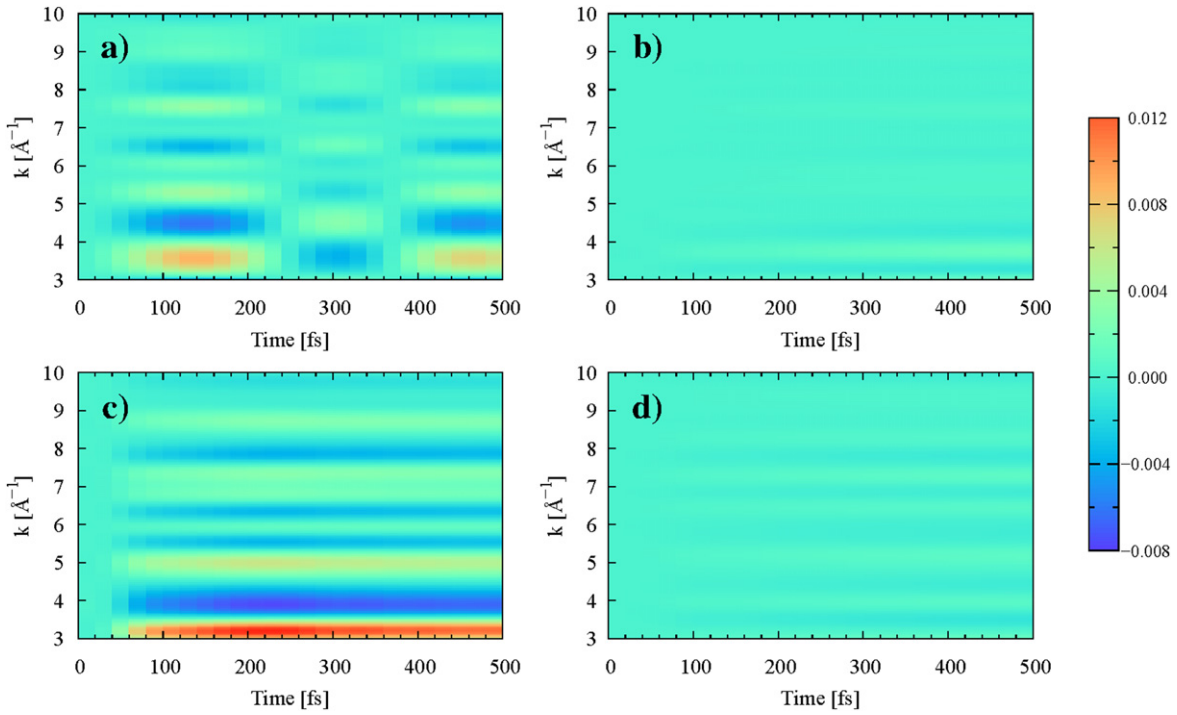

Figure 3. The simulated transient Cu K-edge EXAFS spectrum, $\Delta\chi$, of $[Cu(dmp)_2]^+$ for the first 500 fs after photoexcitation. In each case the spectra are calculated using the nuclear wavepacket dynamics along one degree of freedom; ν_8 (a), ν_{19} (b), ν_{21} (c), ν_{25} (d).

Finally, for both the XAS and XES spectra, the relative energies of the calculated transition are generally well reproduced compared to experiment. However, it is well documented that the absolute transition energies are usually in poor agreement [50]. This failure stems from the approximate exchange description within the exchange-correlation functionals and is associated with the self interaction error [51]. This is usually corrected by applying a constant shift to the spectrum *a posteriori* [52, 53]. In this case, as the spectra presented herein are not directly compared to experimental data, these shifts have not been included.

3. Results

In the following sections, we present the simulations of the EXAFS, pre-edge XANES and XES spectra. Then, using the calculated signal magnitudes, we derive the anticipated feasibility of these techniques to probe the wavepacket dynamics.

3.1. EXAFS

The ground state EXAFS spectrum of $[Cu(dmp)_2]^+$ [54] compared to the spectrum simulated using the ground state wavepacket is shown in figure S1. Although the simulated spectrum is slightly more structured than the experimental spectrum, fairly good agreement between the two is observed with the main features, especially those at low k, well captured. As previously reported [54], this EXAFS spectrum is largely dependent on the Cu–N distance, which is 2.09 Å in the ground state.

Figure 3 shows the transient EXAFS spectra for the first 500 fs of the photoexcited dynamics projected along 4 (ν_8, ν_{19}, ν_{21}, ν_{25}) of the eight nuclear degrees of freedom included in the model Hamiltonian. This shows that two modes, ν_8 and ν_{21}, would be expected to dominate the transient features. The other two modes, ν_{19}, ν_{25} have a weak signal as they are not strongly displaced from their ground state configuration during the dynamics [28]. Of the two active modes, ν_8 is the totally symmetric breathing mode responsible for the contraction of the Cu–N distance in the excited state. This shows an oscillation, caused by a phase shift in the transient EXAFS spectrum, with a period of ~300 fs in good agreement with the wavepacket dynamics reported by Tahara *et al* [55]. In contrast ν_{21}, which is the mode associated with the PJT distortion, exhibits a strong transient signal that is out of phase with the features occurring in the ground state EXAFS spectrum (figure S1), pointing to a damping of the EXAFS features in the excited state. It occurs because the excited state potential along this mode is flatter than the ground state, leading to a nuclear wavepacket that is more spread in the excited state. This additional width has the same dampening effect on the EXAFS spectrum as a Debye-Waller term [56].

Figure 4(a) shows the simulated transient EXAFS spectrum using the nuclear wavepacket dynamics projected in the 2D nuclear coordinate space of ν_8 and ν_{21}. This shows a transient that has its main features out of phase with the ground state spectrum, but which is superimposed with the 300 fs oscillation associated with the wavepacket motion along ν_8. Due to the simplicity of the first coordination sphere, which is the dominant contribution to the EXAFS

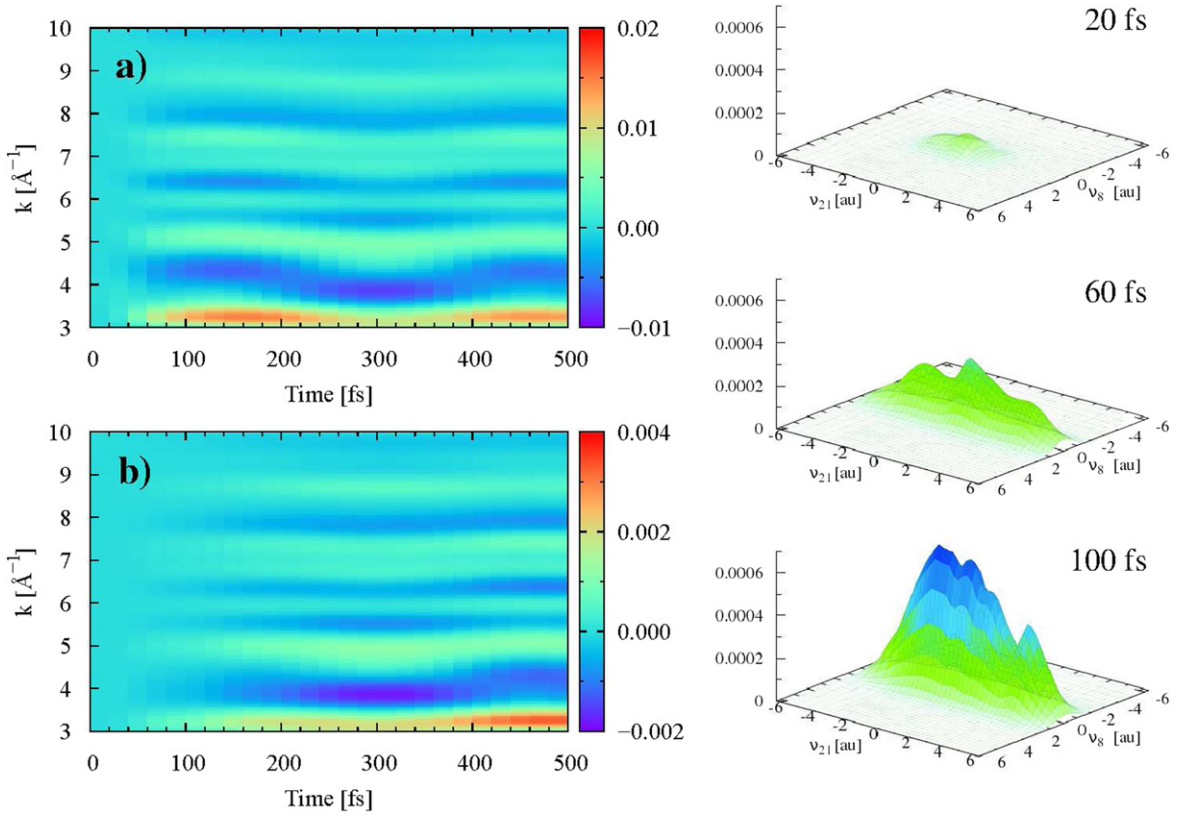

Figure 4. The simulated transient Cu K-edge EXAFS spectrum of $[Cu(dmp)_2]^+$ for the first 500 fs after photoexcitation calculated using the nuclear wavepacket dynamics occurring in the 2D nuclear coordinate space of ν_8 and ν_{21}. (a) The spectrum for the full nuclear wavepacket (b) the spectrum for the wavepacket dynamics in only the lowest triplet (T_1) state. The right hand side shows snapshots of the nuclear wavepacket in the T_1 state along the two modes at 20, 60 and 100 fs.

spectrum, this general structure is repeated at larger photoelectron energies (k), meaning that the experimental spectrum only needs to be recorded to $\sim$5 Å^{-1} ($\sim$9080 eV, $\sim$100 eV above the absorption edge). However, it is noted that in more complicated systems, with a less symmetric first coordination shell around the absorbing atom, different dynamics may well be reflect at different photoelectron energies, especially in the presence of heavier elements that scatter at larger k [57, 58].

As discussed in section 2.2, simulations of the EXAFS spectrum for the different excited states requires only the nuclear geometry. But this is not the case for the pre-edge region of the XAS spectrum and for the XES spectrum. For these cases, we investigate the ultrafast dynamics on the T_1 state only. Consequently to assess the effect of this approximation, figure 4(b) shows the transient EXAFS spectrum using nuclear wavepacket in the 2D nuclear coordinate space of ν_8 and ν_{21}, for which only the wavepacket on the T_1 has been considered. Importantly, the same wavepacket dynamics are observed, although the signal is a factor of $\sim$5 weaker. This is due to the smaller ($<$30%) population (see figure 1) of the T_1 state.

3.2. Pre-edge XAS

Figure 5(a) shows the Cu K-edge pre-edge XANES spectrum in the ground and T_1 states (500 fs after photoexcitation) calculated using the 2D nuclear coordinate space of ν_8 and ν_{21}. The transient spectra simulated at every time-delay (τ) of 20 fs between $\tau = 0$ to 500 fs are shown in figure S2. Ideally, one would wish to simulate the entire XANES spectrum. However, as a result of the difficulties associated with a quantitative description of these transient features [59], a quantitative agreement between the experimental spectrum recorded at a time-delay of 50 ps and the corresponding simulations [54] could not be achieved. Consequently, we focus upon the pre-edge region of the spectrum.

As reported in [54], the transient spectrum (figure 5(a)) shows the two main features, a weak positive feature 8747 eV that corresponds to a 1s $\rightarrow$ 3d transition, and a strong negative feature that corresponds to a loss of intensity of the 1s–4p transition in the ground state spectrum. This latter feature is due to the blue shift of the absorption edge due to the oxidation state change of the metal centre upon population of the MLCT state.

The spectral changes in the transient pre-edge XANES spectra are dominated by the oxidation shift of the absorption edge and the change of the population of the T_1 (see figure S2). As a consequence they do not exhibit any distinct changes associated with the wavepacket dynamics. To remove these two effects, figure 5(b) shows the transient changes occurring in the T_1 state only, i.e. $T_1(\tau$ fs)-T_1(20 fs). Time traces at specific energies are shown in figure 5(c). The time-trace at 8753.5 eV, corresponding to just below the 1s–4p transition in the ground

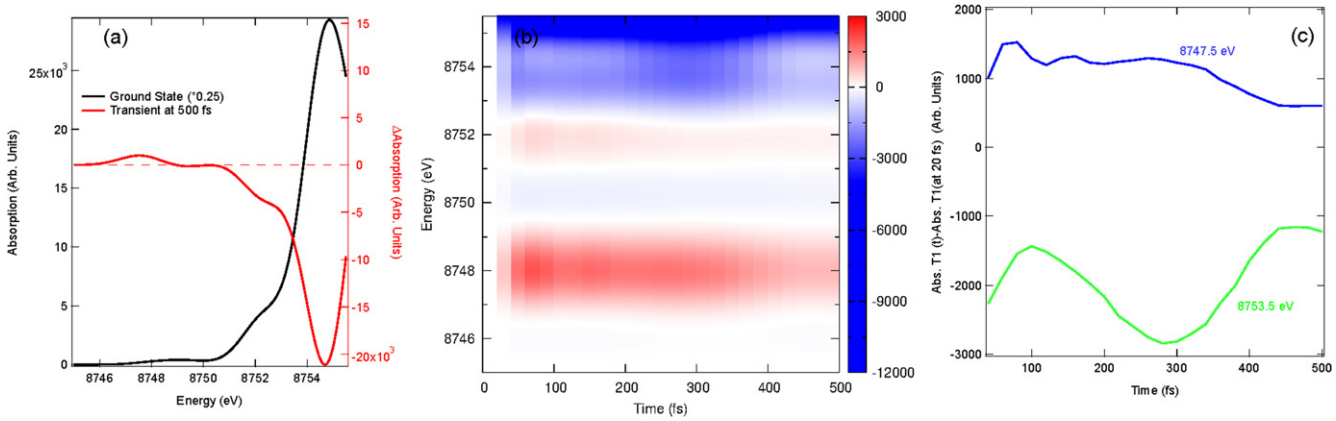

Figure 5. The simulated Cu K-edge pre-edge XANES spectra for the dynamics in the lowest triplet T_1 state. (a) The ground state spectrum (scaled by 0.25) and transient spectrum of the wavepacket in the lowest triplet state 500 fs after photoexcitation (b) the transient changes changes in the lowest triplet state calculated using $T_1(\tau$ fs)-T_1(20 fs) (c) time traces of (b) at 8745.5 and 8753.5 eV.

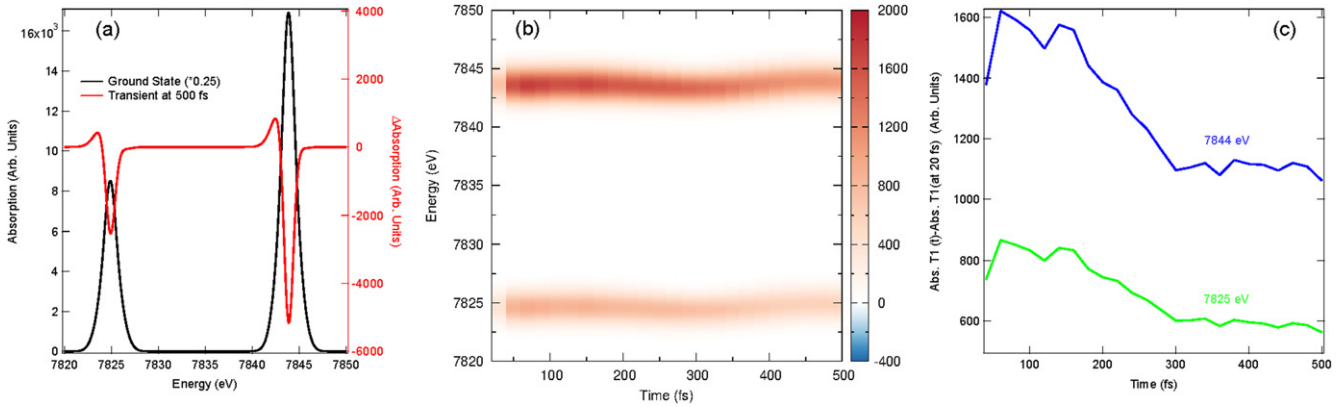

Figure 6. The simulated Cu K$\alpha_{1,2}$ XES spectra for the dynamics in the lowest triplet T_1 state. (a) The ground state spectrum (scaled by 0.25) and transient spectrum of the wavepacket in the lowest triplet state 500 fs after photoexcitation (b) the transient changes changes in the lowest triplet state calculated using $T_1(\tau$ fs)-T_1(20 fs) (c) Time traces of (b) at 7825 and 7844 eV.

state spectrum, captures the oscillatory dynamics observed in the EXAFS spectra and exhibits a signal change ~1%. Importantly, as the main features in the transient spectrum and the vibrational dynamics are unrelated, the energy region most sensitive to the wavepacket dynamics, in this case 8753.5 eV, does not necessarily correspond to the largest changes in the transient spectrum. Given the energy range considered here, we also cannot rule out these changes also occurring at higher energies in the XANES region of the spectrum, however these will be significantly smaller than the transient changes associated with the 1s–4p transition and much closer to those of the EXAFS region.

3.3. X-ray emission

Figure 6(a) shows the K$\alpha_{1,2}$ XES spectra in the ground and 500 fs T_1 transient calculated using the 2D nuclear coordinate space. The transient spectra calculated every 20 fs between $\tau = 0$ and 500 fs are shown in figure S3. The changes are small (~10%) and dominated by a shift in the emission energy associated with the change of spin state compared to the ground state [60]. This dominance of changing spin state is not surprising, as this core to core (2p → 1s) transition is not very sensitive to small changes in the molecular structure or valence electronic structure. Figures 6(b) and (c) again show the transient changes in the T_1 state and time traces at 7825 and 7844 eV. In this case, we do not observe any variations that can be associated with the nuclear wavepacket dynamics.

Figure 7 shows the corresponding plots for the K$\beta_{1,3}$ XES spectra. As this concerns transitions from 3p → 1s, it is likely to be more sensitive to the structural and valence electronic structural changes, especially via the 3p–3d exchange integral [61]. Indeed, while the transient spectra, shown in figure 7(a) is again dominated by an edge shift (the transient spectra calculated every 20 fs between $\tau = 0$ and 500 fs are shown in figure S4), figures 7(b) and (d) reveal weak transient changes in the T_1 state and the 300 fs oscillatory period of the Cu–N totally symmetry stretch is observed. The magnitude of the changes associated with the wavepacket dynamics correspond to a ~0.7% spectral change compared to the ground state spectrum, meaning that it has a similar magnitude change as the transient EXAFS signal.

Finally, figure 8 shows the K$\beta_{2,5}$ XES spectra associated with the femtosecond dynamics in the T_1 state. In contrast to the K$\alpha_{1,2}$ and K$\beta_{1,3}$ XES the stronger effect of the wavepacket

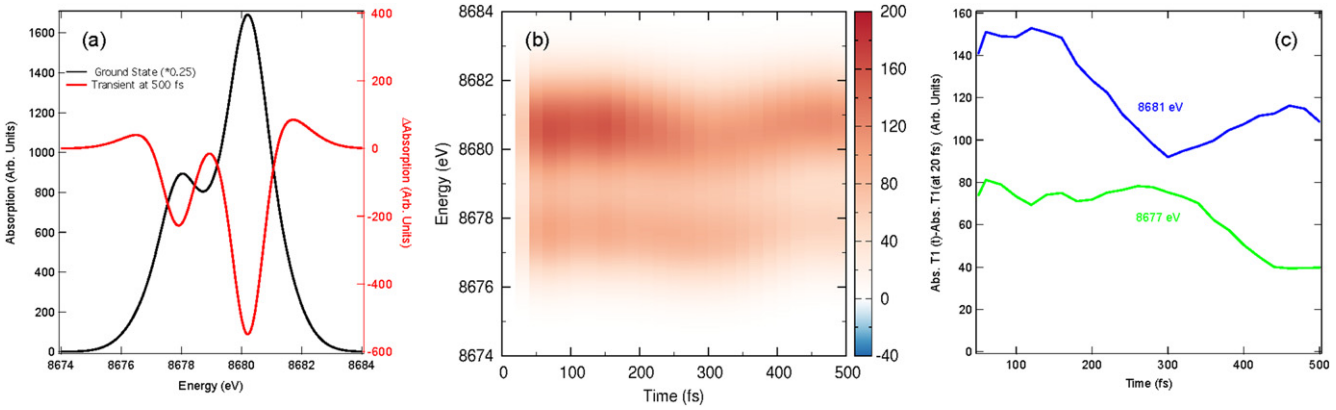

Figure 7. The simulated Cu K$\beta_{1,3}$ XES spectra for the dynamics in the lowest triplet T_1 state. (a) The ground state spectrum (scaled by 0.25) and transient spectrum of the wavepacket in the lowest triplet state 500 fs after photoexcitation (b) the transient changes changes in the lowest triplet state calculated using $T_1(\tau$ fs)-T_1(20 fs) (c) time traces of (b) at 8677 and 8681 eV.

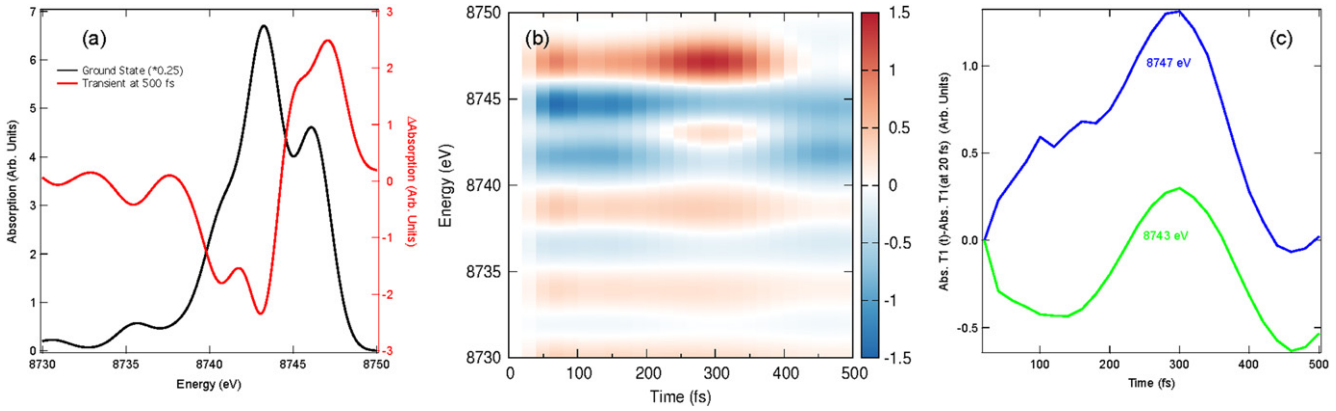

Figure 8. The simulated Cu K$\beta_{2,5}$ XES spectra for the dynamics in the lowest triplet T_1 state. (a) The ground state spectrum (scaled by 0.25) and transient spectrum of the wavepacket in the lowest triplet state 500 fs after photoexcitation (b) The transient changes changes in the lowest triplet state calculated using $T_1(\tau$ fs)-T_1(20 fs) (c) time traces of (b) at 8743 and 8747 eV.

dynamics on the transient signal can be clearly observed in figures 8(b) and (c). This corresponds to a spectral change of ~5% compared to the ground state spectrum and is about an order of magnitude larger than found for EXAFS, K$\alpha_{1,2}$ and K$\beta_{1,3}$ XES. This highlights the distinct advantage and strong signals associated with directly probing the occupied valence density of states. However, the obvious disadvantage of this technique is, as discussed in the next section, the low cross sections, and therefore photon yields, associated with these transitions.

3.4. Numerical examples: feasibility of probing wavepacket dynamics

In the previous sections we have simulated the femtosecond EXAFS, pre-edge XANES and K$\alpha_{1,2}$, K$\beta_{1,3}$ and K$\beta_{2,5}$ XES spectra of photoexcited $[Cu(dmp)_2]^+$ using the nuclear wavepacket dynamics reported in [27, 28]. These have demonstrated that some of the signals (pre-edge XANES, EXAFS, K$\beta_{1,3}$ and K$\beta_{2,5}$) bear characteristics related to the wavepacket dynamics. However, the most crucial aspect of this work, regarding femtosecond laser-pump x-ray-probe experiments being used to investigate such dynamics is the x-ray photon flux required to achieve sufficient sensitivity to resolve these small spectral changes.

Many x-ray spectroscopic measurements are performed in fluorescence yield mode. For spectroscopies based upon the detection of scattered (fluorescent) photons, the spectra are formally represented within second order perturbation theory using the Kramers–Heisenberg equation:

$$F(\Omega,\omega)=\sum_f\sum_n \frac{\overbrace{\left\langle f\left|\hat{H}_{\rm int}\right|n\right\rangle^2}^{\text{Emission}}\overbrace{\left\langle n\left|\hat{H}_{\rm int}\right|i\right\rangle^2}^{\text{Absorption}}}{\left(E_i-E_n+\hbar\Omega\right)^2+\dfrac{\Gamma_n^2}{4}} \times\frac{\Gamma_f/2\pi}{\left(E_i-E_f+\hbar\Omega-\hbar\omega\right)^2+\Gamma_f^2/4}, \quad (1)$$

where $\hbar\Omega$ and $\hbar\omega$ are the incident and emitted photons, respectively and E_i, E_n, E_f are the energies of the initial, intermediate and final states. Γ_n and Γ_f are the lifetime broadening associated with the intermediate and final states. Here, we assume a non-coherent process, in which the absorption matrix elements from initial state i to intermediate

Table 1. The number of x-ray photons ($I^{N\text{pho}}$) and the number (N_{shots}) of x-ray pulses (10^{10} photons per pulse) required to observe the transient $\Delta\chi$ associated with a normal pump–probe signal (signal) and to directly observe the wavepacket dynamics (WP). The photolysis yield f is assumed to be 10% throughout. †: This is only valid for the 1s–4p transition in the XANES region. Other changes are smaller and the pre-edge, being dipole forbidden 1s–3d transitions is significantly smaller and much closer to the spectral changes observed in the EXAFS region of the spectrum.

	Photons out per pulse	$\Delta\chi$ (Signal)	$I^{N\text{pho}}$ (N_{shots})	$\Delta\chi$ (WP)	$I^{N\text{pho}}$ (N_{shots})
TFY XANES	4.0×10^6	0.60†	3.0×10^4 (1)	0.01†	1×10^8 (25)
TFY EXAFS	4.0×10^6	0.01	1.0×10^8 (25)	0.003	1×10^9 (250)
K$\alpha_{1,2}$	6.0×10^3	0.10	1.0×10^6 (170)	—	—
K$\beta_{1,3}$	6.0×10^2	0.20	2.5×10^5 (425)	0.007	2.0×10^8 (3.5×10^5)
K$\beta_{2,5}$	2.0×10^0	0.40	6.3×10^4 (3.2×10^4)	0.050	4×10^6 (2.0×10^6)

state n, mediated by the interaction Hamiltonian $\hat{H}_i$, are weighted by the emission matrix elements [11, 62].

For measurements of the XAS spectra, performed in total fluorescence yield (TFY) mode, the cross section of the absorption matrix element ($\langle n|\hat{H}_{\text{int}}|i\rangle$) at a particular x-ray incident energy is integrated over all of the emission matrix elements ($\langle f|\hat{H}_{\text{int}}|n\rangle$). Consequently, as discrimination of the energy of the emitted photons is not required, one can use a point detector, such as a silicon photodiode [20]. These can be placed close (∼15 mm) to the sample, and can therefore achieve a larger solid angle. Using the relation:

$$\theta = \frac{\pi r_{\text{APD}}^2}{4\pi R^2} \tag{2}$$

and assuming that the detector's active radius, $r_{\text{APD}} = 7$ mm the solid angle (θ) is ∼5%. Given the efficiency of the fluorescence process at Cu K-edge is ∼45% [63] and assuming a detector with a quantum efficiency of ∼0.8 [64, 65], we can combine these three components to yield a loss factor (of the photons in versus the photons out) of 2×10^{-2}.

In contrast, detection of the XES elements is proportional to the cross section of the absorption matrix element ($\langle n|\hat{H}_{\text{int}}|i\rangle$) multiplied by the cross section of the emission line of interest ($\langle f|\hat{H}_{\text{int}}|n\rangle$), i.e. $K\alpha_{1,2}$, $K\beta_{1,3}$. Consequently, the photon yield for each spectrum will be significantly lower making it harder to achieve a large signal to noise ratio (SNR) for these photon hungry techniques. In addition, for these experiments the XES spectrometer is further away from the sample causing additional losses and a smaller solid angle [60, 66]. For each emission line of interest, the fluorescence efficiency are Cu K$\alpha_{1,2}$ = 0.3, Cu K$\beta_{1,3}$-edge = 0.03 and Cu K$\beta_{2,5}$-edge = 0.00001 [63, 66]. Consequently given a reduced solid angle arising from the larger sample detector distance of $\theta\sim$ 0.04% (∼5 millisteradians) [66, 67], the x-ray attenuation in air due to the larger distance from the detector [68], which is assumed to be 0.3, the total losses are Cu K$\alpha_{1,2}$ -edge = 3.0×10^{-5}, Cu K$\beta_{1,3}$-edge = 3.0×10^{-6} and Cu K$\beta_{2,5}$-edge = 9.6×10^{-9}.

Assuming a 100 μm thick jet of 25 mM solution, the absorbed fraction of photons, according to the Beer–Lambert law is ∼2%. It is stressed that this approximation is only strictly valid for solvents containing light elements (e.g., water, acetonitrile, hexane) and may change for heavier solvents, like CCl_4 [65]. With these conditions in mind, given 10^{10} photons per pulse achievable for the monochromatic mode of the Linac coherent light source (LCLS) [69], the number of useful photons per pulse detected (see table 1), i.e. once the loss factors have been included, is: 4×10^6 (TFY), 6×10^3 (Cu K$\alpha_{1,2}$), 6.0×10^2 (Cu K$\beta_{1,3}$) and 2.0×10^0 (Cu K$\beta_{2,5}$).

In an experiment, provided that most of the electronic noise is suppressed, the detection sensitivity can be close to the shot-noise limit. This inherent noise is given as $\sqrt{N}$, where N is the signal, i.e. the number of photons detected. The SNR is therefore given SNR = N/$\sqrt{N}$. Using these boundary conditions, table 1 shows the number of x-ray photons, and consequently of x-ray pulses, required to measure with a SNR = 10 for (i) a transient x-ray spectroscopic signal and (ii) the wavepacket dynamics. The number of x-ray photons ($I^{N\text{pho}}$) required to measure a given signal scales as [65]:

$$I^{N\text{pho}} \propto \left[\frac{SNR}{f \cdot \Delta\chi}\right]^2 \tag{3}$$

where $\Delta\chi$ is the signal change and f is the photolysis yield assumed to be 10% throughout. Using $I^0 = 10^{10}$ as the incoming x-ray intensity (number of photons per pulse), the loss factor (L) and the fraction of absorbed photons (μ_A), we can use equation (3) to estimate the number of x-ray pulses (N_{shots}) required with:

$$N_{\text{shots}} = \frac{I^{N\text{pho}}}{I_0 \cdot \mu_A \cdot L}. \tag{4}$$

Using equations (3) and (4), table 1 shows that to record a transient signal pump–probe using TFY XANES or TFY EXAFS requires ∼3.0×10^4 and ∼1.0×10^8 photons, respectively. Given that the number of detected photons/pulse detected is 4×10^6, this makes it plausible for each data point of TFY XANES to be recorded with a SNR = 10 within a single X-FEL pulse. TFY EXAFS requires ∼25 x-ray pulses, however this still means that each data point can be collected with <1s of acquisition time (assuming a 100 Hz repetition rate). In contrast, due to smaller $\Delta\chi$ associated with resolving the spectral fluctuations of wavepacket dynamics a

larger number of photons is required. Indeed, to achieve a SNR = 10, for TFY XANES and TFY EXAFS each data point would be expected to require ~25 and ~250 x-ray pulses, respectively. Importantly, this is still achievable within a reasonable data acquisition time (<4s per data point).

Table 1 also shows the number of photons required to achieve a transient signal, $\Delta\chi$ for K$\alpha_{1,2}$, K$\beta_{1,3}$ and K$\beta_{2,5}$ XES. While these photon hungry techniques are difficult to implement in a time-resolved manner at 3rd generation synchrotrons [60, 67], the increased photon flux associated with the X-FELs makes these feasible in the sub-ps regime. Indeed, for the hardest case, K$\beta_{2,5}$ XES, it is expected that $\sim 3.2 \times 10^4$ x-ray pulses per data point is required. Given the repetition rate of X-FELs (~100 Hz), this would require acquisition times of ~10–20 min per data point. For these experiments the potentially high x-ray fluency and repetition rate of the European X-FEL could make such measurements significantly easier [70]. However, table 1 shows that although measuring the transient signal is possible even for K$\beta_{2,5}$ XES, the number of x-ray pulses, $\sim 10^{5-6}$ required to achieve sufficient SNR to observe the wavepacket dynamics with these spectroscopies makes them completely unfeasible (~6 hours per data point at 100 Hz).

4. Discussions and conclusions

Ultrafast time-resolved linear and non-linear optical spectroscopies have a strong history of providing important insight into photoexcited dynamics within the femtosecond regime. Owing to the development of the X-FELs, these dynamics can now also be observed in the short-wavelength regime and provide direct snapshots of interatomic distances and changes in charge distribution of molecules. These techniques hold great promise of yielding important new insight into fundamental dynamical processes such as vibrational excitation, bond formation and breaking, relaxation, and time-dependent solvation processes.

In this paper we have used wavepacket dynamics simulations to predict femtosecond EXAFS, pre-edge XANES, K$\alpha_{1,2}$, K$\alpha_{1,3}$ and K$\beta_{2,5}$ XES spectra. These have demonstrated that for the present system, femtosecond pre-edge XANES, EXAFS, K$\beta_{1,3}$ and K$\beta_{2,5}$ XES spectra all reveal information about the wavepacket dynamics. However using realistic experimental parameters, while it will be possible to record a signal capturing the strongest transient changes for all of the spectroscopies studies herein, we have demonstrated that the wavepacket dynamics can only be observed experimentally within realistic acquisition times for XANES and EXAFS, as the small cross section associated with K$\beta_{1,3}$ and K$\beta_{2,5}$ XES makes the number of x-ray pulses required unfeasible.

In the present study we have not considered L-edge spectroscopy. However recent work has demonstrated that it is possible to record high quality L-edge spectra of dilute 3d transition metals using a high transmission zone-plate spectrometer implemented at the LCLS. [71]. Although the L-edges have a smaller fluorescence yield (~1%), these transitions (2p–3d) could be a interesting alternative approach that should also be explored.

Importantly, in terms of a general feasibility, the transient signals for the present case $[Cu(dmp)_2]^+$ are dominated by an oxidation shift associated with the charge transfer of an electron from the metal to the ligands upon excitation. As this has no correspondence with the wavepacket dynamics, the changes associated with these vibrational coherences will be a small change on top of the large underlying transient of the edge shift. This means that resolving the wavepacket dynamics for the present system represents a challenging case. Given that it remains possible, this holds significant promise for future experiments in this area. It should be stressed that as the main features in the transient spectrum and the vibrational dynamics are unrelated, the energy region most sensitive to the wavepacket dynamics does not necessarily correspond to the largest changes in the transient spectrum making it important to record the whole spectrum at each time-delay and not just a time scan at one particular energy. For other cases, such as $[Fe(bpy)_3]^{2+}$ [15, 60, 72–74] determining the wavepacket dynamics could be expected to be easier. In this case, the transient spectrum is not dominated by a feature unrelated to the vibrational coherences. Instead, here the wavepacket dynamics reported by Chergui and co-workers [75] occurs along this Fe–N coordinate, which is also responsible for the principal transient changes in the Fe K-edge XAS spectrum. In this case the wavepacket dynamics would therefore be expected to yield larger changes making observing these dynamics easier. This highlights the strong emphasis that should be placed upon fully understanding the dominant contributions to a transient signal at longer times (i.e. using a 3rd generation synchrotrons) before determining if a particular experiment is possible.

Acknowledgments

We thank the Swiss National Science Foundation (Grant 200021–137717) and the NCCR MUST for funding.

References

[1] Zewail A H 1988 Laser femtochemistry *Science* **242** 1645–53
[2] Mukamel S 1995 *Principles of Nonlinear Optical Spectroscopy* (USA: Oxford University Press)
[3] Reis D A and Lindenberg A M 2007 Ultrafast x-ray scattering in solids *Light Scattering In Solids: IX* **vol 108** pp 371–422
[4] Elsaesser T and Woerner M 2010 Photoinduced structural dynamics of polar solids studied by femtosecond x-ray diffraction *Acta Crystallogr.* A **66** 168–78
[5] Johnson S L, Beaud P, Vorobeva E, Milne C J, Murray E D, Fahy S and Ingold G 2010 Non-equilibrium phonon dynamics studied by grazing-incidence femtosecond x-ray crystallography *Acta Crystallogr.* A **66** 157–67
[6] Sciaini G and Miller R J D 2011 Femtosecond electron diffraction: heralding the era of atomically resolved dynamics *Rep. Prog. Phys.* **74** 096101

[7] Chergui M and Zewail A H 2009 Electron and x-ray methods of ultrafast structural dynamics: advances and applications *ChemPhysChem* **10** 28–43

[8] Penfold T J, Milne C J and Chergui M 2013 Recent advances in ultrafast x-ray absorption spectroscopy of solutions *Adv. Chem. Phys.* **153** 1–41

[9] Bressler C and Chergui M 2010 Molecular structural dynamics probed by ultrafast x-ray absorption spectroscopy *Annu. Rev. Phys. Chem.* **61** 263–82

[10] Chen L X 2001 Probing transient molecular structures with time-resolved pump/probe XAFS using synchrotron x-ray sources *J. Electron Spectrosc. Relat. Phenom.* **119** 161–74

[11] Milne C J, Penfold T J and Chergui M 2014 Recent experimental and theoretical developments intime-resolved x-ray spectroscopies *Coord. Chem. Rev.*

[12] Zewail A H 2006 4D ultrafast electron diffraction, crystallography, and microscopy *Annu. Rev. Phys. Chem.* **57** 65–103

[13] van der Veen R M, Penfold T J and Zewail A H 2015 Ultrafast core-loss spectroscopy in four-dimensional electron microscopy *Struct. Dyn.* **2** 024302

[14] Schoenlein R W, Chattopadhyay S, Chong H H W, Glover T E, Heimann P A, Shank C V, Zholents A A and Zolotorev M S 2000 Generation of femtosecond pulses of synchrotron radiation *Science* **287** 2237–40

[15] Bressler C *et al* 2009 Femtosecond XANES study of the light-induced spin crossover dynamics in an iron(II) complex *Science* **323** 489–92

[16] Huse N, Cho H, Hong K, Jamula L, de Groot F M F, Kim T K, McCusker J K and Schoenlein R W 2011 Femtosecond soft x-ray spectroscopy of solvated transition-metal complexes: deciphering the interplay of electronic and structural dynamics *J. Phys. Chem. Lett.* **2** 880–4

[17] Pham V-T *et al* 2011 Probing the transition from hydrophilic to hydrophobic solvation with atomic scale resolution *J. Am. Chem. Soc.* **133** 12740–8

[18] Cavalleri A, Rini M, Chong H H W, Fourmaux S, Glover T E, Heimann P A, Kieffer J C and Schoenlein R W 2005 Band-selective measurements of electron dynamics in vo 2 using femtosecond near-edge x-ray absorption *Phys. Rev. Lett.* **95** 067405

[19] Khan S 2008 Free-electron lasers *J. Mod. Opt.* **55** 3469–512

[20] Lemke H T *et al* 2013 Femtosecond x-ray absorption spectroscopy at a hard x-ray free electron laser: application to spin crossover dynamics *J. Phys. Chem.* A **117** 735–40

[21] Zhang W *et al* 2014 Tracking excited-state charge and spin dynamics in iron coordination complexes *Nature* **509** 345–8

[22] Cammarata M *et al* 2014 Sequential activation of molecular breathing and bending during spin-crossover photoswitching revealed by femtosecond optical and x-ray absorption spectroscopy *Phys. Rev. Lett.* **113** 227402

[23] Ogi Y *et al* 2015 Ultraviolet photochemical reaction of [fe (iii) (c2o4) 3] 3- in aqueous solutions studied by femtosecond time-resolved x-ray absorption spectroscopy using an x-ray free electron laser *Struct. Dyn.* **2** 034901

[24] Wernet P h *et al* 2015 Orbital-specific mapping of the ligand exchange dynamics of Fe(CO)5 in solution *Nature* **520** 78–81

[25] Stolow A, Bragg A E and Neumark D M 2004 Femtosecond time-resolved photoelectron spectroscopy *Chem. Rev.* **104** 1719–58

[26] Mukamel S 1990 Femtosecond optical spectroscopy: a direct look at elementary chemical events *Annu. Rev. Phys. Chem.* **41** 647–81

[27] Capano G, Penfold T J, Rothlisberger U and Tavernelli I 2014 A vibronic coupling Hamiltonian to describe the ultrafast excited state dynamics of a Cu(I)-phenanthroline complex *Chimia* **68** 227–30

[28] Capano G, Chergui M, Rothlisberger U, Tavernelli I and Penfold T J 2014 A quantum dynamics study of the ultrafast relaxation in a prototypical cu(i)-phenanthroline *J. Phys. Chem.* A 0(ja):null

[29] Chen L X, Shaw G B, Novozhilova I, Liu T, Jennings G, Attenkofer K, Meyer G J and Coppens P 2003 MLCT state structure and dynamics of a copper(I) diimine complex characterized by pump–probe x-ray and laser spectroscopies and DFT calculations *J. Am. Chem. Soc.* **125** 7022–34

[30] Siddique Z A, Yamamoto Y, Ohno T and Nozaki K 2003 Structure-dependent photophysical properties of singlet and triplet metal-to-ligand charge transfer states in copper(I) bis (diimine) compounds *Measurement* **42** 6366–78

[31] Shaw G B, Grant C D, Shirota H, CASTNER E W, Meyer G J and Chen L X 2007 Ultrafast structural rearrangements in the MLCT excited state for copper(I) bis-phenanthrolines in solution *J. Am. Chem. Soc.* **129** 2147–60

[32] Iwamura M, Takeuchi S and Tahara T 2007 Real-time observation of the photoinduced structural change of bis(2, 9-dimethyl-1, 10-phenanthroline)copper(I) by femtosecond fluorescence spectroscopy: a realistic potential curve of the Jahn–Teller distortion *J. Am. Chem. Soc.* **129** 5248–56

[33] Iwamura M, Watanabe H, Ishii K, Takeuchi S and Tahara T 2011 Coherent nuclear dynamics in ultrafast photoinduced structural change of Bis (diimine) copper (I) complex *J. Am. Chem. Soc.* **133** 7728

[34] Iwamura M, Takeuchi S and Tahara T 2014 Substituent effect on the photoinduced structural change of Cu(I) complexes observed by femtosecond emission spectroscopy *Phys. Chem. Chem. Phys.* **16** 4143–54

[35] Meyer H-D, Manthe U and Cederbaum L S 1990 The multi-configurational time-dependent Hartree approach *Chem. Phys. Lett.* **165** 73–78

[36] Beck M H, Jäckle A, Worth G A and Meyer H-D 2000 The multiconfiguration time-dependent Hartree method: a highly efficient algorithm for propagating wavepackets *Phys. Rep.* **324** 1–105

[37] Köppel H, Domcke W and Cederbaum L S 1984 Multimode molecular dynamics beyond the Born–Oppenheimer approximation **57** 59–246

[38] Josefsson I, Kunnus K, Schreck S, Föhlisch A, de Groot F, Wernet P and Odelius M 2012 *Ab initio* calculations of x-ray spectra: atomic multiplet and molecular orbital effects in a multiconfigurational scf approach to the l-edge spectra of transition metal complexes *J. Phys. Chem. Lett.* 3565–70

[39] Besley N A, Gilbert A T B and Gill P M W 2009 Self-consistent-field calculations of core excited states *J. Chem. Phys.* **130** 124308

[40] Besley N A 2012 Equation of motion coupled cluster theory calculations of the x-ray emission spectroscopy of water *Chem. Phys. Lett.* **542** 42–46

[41] Rehr J J, Kas J J, Prange M P, Sorini A P, Takimoto Y and Vila F 2009 *Ab initio* theory and calculations of x-ray spectra *C. R. Phys.* **10** 548

[42] Beckwith M A, Roemelt M, Collomb M, DuBoc C, Weng T-C, Bergmann U, Glatzel P, Neese F and DeBeer S 2011 Manganese kβ x-ray emission spectroscopy as a probe of metal–ligand interactions *Inorg. Chem.* **50** 8397–409

[43] Lee N, Petrenko T, Bergmann U, Neese F and DeBeer S 2010 Probing valence orbital composition with iron kβ x-ray emission spectroscopy *J. Am. Chem. Soc.* **132** 9715–27

[44] Neese F 2012 The ORCA program system *Wiley Interdiscip. Rev.-Comput. Mol. Sci.* **2** 73–78

[45] Becke A D 1988 Density-functional exchange-energy approximation with correct asymptotic behavior *Phys. Rev.* A **38** 3098–100

[46] Perdew J P 1986 Density-functional approximation for the correlation-energy of the inhomogeneous electron-gas *Phys. Rev.* B **33** 8822–4

[47] Schäfer A, Horn H and Ahlrichs R 1992 Fully optimized contracted gaussian basis sets for atoms li to kr *J. Chem. Phys.* **97** 2571–7
[48] Weigend F and Ahlrichs R 2005 Balanced basis sets of split valence, triple zeta valence and quadruple zeta valence quality for h to rn: design and assessment of accuracy *Phys. Chem. Chem. Phys.* **7** 3297–305
[49] Hess B A, Marian C M, Wahlgren U and Gropen O 1996 A mean-field spin–orbit method applicable to correlated wavefunctions *Chem. Phys. Lett.* **251** 365–71
[50] Stener M 2003 Time dependent density functional theory of core electrons excitations *Chem. Phys. Lett.* **373** 115–23
[51] Besley N A, Peach M J G and Tozer D J 2009 Time-dependent density functional theory calculations of near-edge x-ray absorption fine structure with short-range corrected functionals *Phys. Chem. Chem. Phys.* **11** 10350
[52] DeBeer-George S, Petrenko T and Neese F 2008 Prediction of iron K-edge absorption spectra using time-dependent density functional theory *J. Phys. Chem.* A **112** 12936–43
[53] Capano G, Penfold T J, Besley N A, Milne C J, Reinhard M, Rittmann-Frank H, Glatzel P, Abela R, Rothlisberger U, Chergui M and Tavernelli I 2013 The role of Hartree–Fock exchange in the simulation of x-ray absorption spectra: a study of photoexcited $[Fe(bpy)_3]^{2+}$ *Chem. Phys. Lett.* **580** 179–84
[54] Penfold T J *et al* 2013 Solvent-induced luminescence quenching: static and time-resolved x-ray absorption spectroscopy of a copper(I) phenanthroline complex *J. Phys. Chem.* A **117** 4591–601
[55] Iwamura M, Takeuchi S and Tahara T 2015 Ultrafast excited-state dynamics of copper (i) complexes *Acc. Chem. Res.* **48** 782–91
[56] Jackson B and Metiu H 1985 An examination of the use of wave packets for the calculation of atom diffraction by surfaces *J. Chem. Phys.* **82** 5707–16
[57] Koningsberger D C, Mojet B L, van Dorssen G E and Ramaker D E 2000 XAFS spectroscopy; fundamental principles and data analysis *Top. Catal.* **10** 143–55
[58] Penfold T J, Tavernelli I, Milne C J, Reinhard M, el Nahhas A, Rafael Abela U, Rothlisberger and Chergui M 2013 A wavelet analysis for the x-ray absorption spectra of molecules *J. Chem. Phys.* **138** 014104
[59] Rehr J J and Albers R C 2000 Theoretical approaches to x-ray absorption fine structure *Rev. Mod. Phys.* **72** 621–54
[60] Vankó G *et al* 2013 Spin-state studies with XES and RIXS: From static to ultrafast *J. Electron Spectrosc. Relat. Phenom.* **188** 166–71
[61] de Groot F 2001 High-resolution x-ray emission and x-ray absorption spectroscopy *Chem. Rev.* **101** 1779–808
[62] de Groot F and Kotani A 2008 *Core Level Spectroscopy of Solids* (Boca Raton, FL: CRC Press)
[63] Krause M O 1979 Natural widths of atomic K and L levels, Ka x-ray lines and several KLL Auger lines *J. Phys. Chem. Ref. Data* doi:10.1063/1.555595
[64] Gawelda W 2006 Time-resolved x-ray absorption spectroscopy of transition metal complexes *EPFL Thesis* (*November 2006*) pp 1–307
[65] Bressler C and Chergui M 2004 Ultrafast x-ray absorption spectroscopy *Chem. Rev.* **104** 1781–812
[66] Szlachetko J *et al* 2012 A von Hamos x-ray spectrometer based on a segmented-type diffraction crystal for single-shot x-ray emission spectroscopy and time-resolved resonant inelastic x-ray scattering studies *Rev. Sci. Instrum.* **83** 103105
[67] March A M *et al* 2015 Feasibility of valence-to-core x-ray emission spectroscopy for tracking transient species *J. Phys. Chem.* C
[68] Bergmann U and Glatzel P 2009 X-ray emission spectroscopy *Photosynth. Res.* **102** 255–66
[69] Bozek J D 2009 Amo instrumentation for the lcls x-ray fel *Eur. Phys. J.—Spec. Top.* **169** 129–32
[70] Altarelli M *et al* 2006 The european x-ray free-electron laser *Technical Design Report, DESY* vol 97 p 2006
[71] Mitzner R *et al* 2013 L-edge x-ray absorption spectroscopy of dilute systems relevant to metalloproteins using an x-ray free-electron laser *J. Phys. Chem. Lett.* **4** 3641–7
[72] Cannizzo A, Milne C J, Consani C, Gawelda W, Ch Bressler F, van Mourik and Chergui M 2010 Light-induced spin crossover in Fe(II)-based complexes: the full photocycle unraveled by ultrafast optical and x-ray spectroscopies *Coord. Chem. Rev.* **254** 2677–86
[73] Gawelda W, Pham V T, van der Veen R M, Grolimund D, Rafael Abela M, Chergui and Bressler C 2009 Structural analysis of ultrafast extended x-ray absorption fine structure with subpicometer spatial resolution: application to spin crossover complexes *J. Chem. Phys.* **130** 124520
[74] Haldrup K *et al* 2012 Guest-host interactions investigated by time-resolved x-ray spectroscopies and scattering at MHz rates: solvation dynamics and photoinduced spin transition in aqueous $Fe(bipy)_3^{2+}$ *J. Phys. Chem.* A **116** 9878–87
[75] Consani C, Prémont-Schwarz M, ElNahhas A, Bressler C, van Mourik F, Cannizzo A and Chergui M 2009 Vibrational coherences and relaxation in the high-spin state of aqueous $[Fe^{II}(bpy)_3]^{2+}$ *Angew. Chem., Int. Ed. Engl.* **48** 7184–7